RESOURCESAT-1 GEOMETRIC ACCURACY ASSESSMENT

James Lutes
Geodetic Systems Specialist
Space Imaging
12076 Grant Street, Thornton, CO 80241
jlutes@spaceimaging.com

ABSTRACT

RESOURCESAT-1, launched in October 2003, is the latest of the Indian Remote Sensing series of satellites built by the Indian Space Research Organisation. RESOURCESAT-1, also known as IRS-P6, continues and extends the capabilities of the IRS-1C and IRS-1D satellites. The satellite contains three different imaging sensors: LISS-IV, with a ground sampling distance (GSD) of 5.8 meters; LISS-III, with a GSD of 23.5 meters; and AWiFS, with a GSD of 56 meters at nadir.

This paper provides an initial geometric accuracy assessment of the different RESOURCESAT-1 sensors, both with and without ground control. Techniques for recovering imaging geometry from the provided sensor metadata are also discussed, as well as recommended procedures for block adjustment of RESOURCESAT-1 imagery.

INTRODUCTION

On October 17, 2003, the Indian Space Research Organisation (ISRO) launched RESOURCESAT-1 into orbit from its launch facility in Sriharikota, India (ISRO, 2003a). This satellite, the tenth in ISRO's Indian Remote Sensing (IRS) series, is meant to continue the imaging capabilities of the earlier IRS-1C and IRS-1D sensors while offering improved spatial and radiometric resolution over its predecessors.

Space Imaging, the exclusive distributor of RESOURCESAT-1 imagery and satellite access outside India, launched commercial sales of RESOURCESAT-1 data products in August 2004. Imagery from the three RESOURCESAT-1 imaging sensors is offered in a number of different data formats and processing levels, meaning that customers have a choice to make as to what combination of processing level and data format best suits their needs. For customers who wish to perform further photogrammetric processing of RESOURCESAT-1 imagery, this choice is particularly important, as commercial software support for RESOURCESAT-1 imagery is presently quite limited.

In addition to providing an overview of the RESOURCESAT-1 imaging platform and the various data products and processing levels available, this paper presents an assessment of the positional accuracy achievable with RESOURCESAT-1 imagery. Algorithms are also presented to illustrate how the user can take advantage of sensor metadata provided with LGSOWG format imagery products in order to recover the view geometry for further photogrammetric processing.

PLATFORM DESCRIPTION

The RESOURCESAT-1 payload includes three imaging sensors: LISS-IV, with a ground sampling distance (GSD) of 5.8 meters; LISS-III, with a GSD of 23.5 meters; and AWiFS, with a GSD of 56 meters at nadir. This is similar to the complement of sensors onboard IRS-1C and IRS-1D (NRSA, 1995; NRSA, 1997), which were launched in 1995 and 1997 respectively, but with numerous design improvements. This section describes some of the important characteristics of the RESOURCESAT-1 imaging sensors.

LISS-IV

The Linear Imaging Self Scanner IV (LISS-IV) is the highest-resolution imaging sensor on RESOURCESAT-1, offering a GSD of 5.8 meters at nadir. While IRS-1C and IRS-1D contain a single panchromatic sensor at this resolution, LISS-IV can operate in three spectral bands (green, red, and near-infrared). Some of the important technical characteristics of LISS-IV are listed in Table 1 below. In some cases, values listed in Table 1 diverge from

those published in the *IRS-P6 Data Users' Handbook* (ISRO, 2003b); in these cases, the listed value has been obtained from metadata delivered with LISS-IV imagery rather than from the published specifications.

Table 1. LISS-IV sensor specifications

GSD:	5.8 m at nadir		
Swath width:	70 km (MONO mode), 23 km (Multispectral mode)		
Spectral bands:	3		
Approx. focal length:	982 mm		
	Band 2 (green)	**Band 3 (red)**	**Band 4 (near-infrared)**
Sensitivity range:	520-590 nm	620-680 nm	770-860 nm
Quantization:	10 bits (7 bits transferred)	10 bits (7 bits transferred)	10 bits (7 bits transferred)
Array width:	12000 pixels	12000 pixels	12000 pixels
Detector size:	7×7 μm	7×7 μm	7×7 μm

LISS-IV is a pushbroom sensor, as are LISS-III and AWiFS. The 12000 pixel CCD array for each band is separated into odd and even pixels, arranged in two rows with a distance of 35 microns (5 scan lines) between them. A single telescope and lens assembly is used for all three bands; band 3 (red) is placed closest to nadir, while band 2 looks ahead and band 4 looks behind the satellite velocity vector (ISRO, 2003b).

As with IRS-1C and IRS-1D, the LISS-IV sensor has cross-track steering capability of ±26º from nadir, allowing the collection of cross-track stereo images or simply more frequent coverage of a given area of interest. Along-track stereo is planned for the upcoming CARTOSAT-1 satellite, scheduled for launch in the near future (NRSA, 2004).

LISS-IV collects imagery in one of two different modes: monochromatic (Mono) or multispectral (Mx). In Mono mode, the full 12000 pixel array of one band is used to collect a swath width of 70 km. Any one of the three bands can be employed for Mono mode collection, although the red band is normally used because it is closest to nadir. In multispectral mode, 4000 pixels are collected from each of the three bands. Any pixel number from 1 to 8000 can be chosen as the start of the 4000-pixel subset, meaning that the 23-kilometer wide multispectral scene can fall anywhere within the Mono 70 km footprint.

As indicated in Table 1, the LISS-IV image data is digitized to 10 bits onboard the satellite but only 7 bits are transferred from satellite to ground. The selection of which 7 bits to transfer from the 10-bit signal is performed by the satellite operator during collection tasking. Sensor metadata provided with the image product indicates what 'gain' setting (i.e., bit selection) was used for the scene.

LISS-III

LISS-III is a medium resolution sensor, collecting imagery in four spectral bands at a GSD of 23.5 meters. LISS-III is not steerable, so imagery is always collected at nadir. Table 2 lists the main characteristics of LISS-III.

Table 2. LISS-III sensor specifications

GSD:	23.5 m at nadir			
Swath width:	141 km			
Spectral bands:	4			
	Band 2 (green)	**Band 3 (red)**	**Band 4 (NIR)**	**Band 5 (SWIR)**
Sensitivity range:	520-590 nm	620-680 nm	770-860 nm	1550-1700 nm
Quantization:	7 bits	7 bits	7 bits	10 bits (7 bits transferred)
Array width:	6000 pixels	6000 pixels	6000 pixels	6000 pixels
Detector size:	10 μm cross-track 7 μm along-track	10 μm cross-track 7 μm along-track	10 μm cross-track 7 μm along-track	13×13 μm
Approx. focal length:	347.5 mm	347.5 mm	347.5 mm	451.6 mm

The main difference between this model of LISS-III sensor and the version onboard IRS-1C and IRS-1D is the improved spatial resolution of the SWIR band; the current SWIR-band sensor has a GSD of 23.5 meters, while the IRS-1C and IRS-1D SWIR sensor has a GSD of 70.5 meters (NRSA, 1995; NRSA, 1997). The SWIR detector also

has an odd/even pixel stagger like that of LISS-IV, with a spacing of approximately 2 scan lines between odd and even pixels.

The LISS-III camera uses four separate, axis-aligned telescope assemblies to collect the different spectral bands. As a result, the same point on the ground is imaged nearly simultaneously by all bands. This is different from the case of LISS-IV, which has a timelag of more than two seconds between band 2 and band 4 (ISRO, 2003b).

AWiFS

The Advanced Wide Field Sensor (AWiFS), as the name implies, collects a wide swath of 740 km. AWiFS realizes its wide field of view by employing two separate sensor modules (AWiFS-A and AWiFS-B) tilted by 11.94º to the left and right of nadir (ISRO, 2003b). The two modules have a small overlap of coverage in the center, approximately 7 kilometers.

Table 3 lists the main technical specifications of AWiFS. The sensors are very similar to LISS-III (in fact, they use the same type of CCD arrays), but AWiFS has a shorter focal length and increased radiometric resolution.

Table 3. AWiFS sensor specifications

GSD:	56 m at nadir; 70 m at edge of scene			
Swath width:	370 km for each camera (740 km combined)			
Spectral bands:	4			
	Band 2 (green)	**Band 3 (red)**	**Band 4 (NIR)**	**Band 5 (SWIR)**
Sensitivity range:	520-590 nm	620-680 nm	770-860 nm	1550-1700 nm
Quantization:	10 bits	10 bits	10 bits	10 bits
Array width:	6000 pixels	6000 pixels	6000 pixels	6000 pixels
Detector size:	10 µm cross-track 7 µm along-track	10 µm cross-track 7 µm along-track	10 µm cross-track 7 µm along-track	13×13 µm
Approx. focal length:	139.5 mm	139.5 mm	139.5 mm	181.3 mm

DATA PRODUCTS

A variety of different processing levels and data formats are available for RESOURCESAT-1 imagery, and users must choose the appropriate combination to suit their needs. In practice, this is often dictated by the level of support offered by commercial software vendors for the product and by the amount of effort required to generate the desired end product from the imagery.

In the interest of brevity, not all processing levels and data formats will be discussed here; the reader is referred to ISRO (2003b) for details. However, important characteristics of the most common items will be outlined in the following sections. The products described here reflect offerings from Space Imaging only and may not represent the product suite available from other vendors.

Processing Levels

The three basic processing levels are Radiometric, Geo and Orthorectified. Of these three, the Radiometric processing level is not offered as a standard product due to properties (discussed later) that make it difficult for most users to process the data. However, it is the simplest type of product available, and the minimum possible geometric corrections have been applied to the data. The only corrections performed are detector normalization, failed detector correction, stagger correction, and line loss correction (ISRO, 2003b). These are described below.

1. ***Detector normalization.*** Detector normalization involves application of gain and bias values to account for the differing response of each detector; this removes the appearance of striping in the imagery and results in an image for which a single set of Digital Number (DN)-to-radiance conversion coefficients can be provided.
2. ***Failed detector correction.*** If a detector in the CCD array has failed or is not working properly, a value is interpolated from the two neighboring working detectors. This correction is performed if no more than two adjacent detectors require interpolation.
3. ***Stagger correction.*** The three bands of LISS-IV and the SWIR band of LISS-III and AWiFS have staggered even/odd detectors, as mentioned in the previous section. One-dimensional cubic convolution

resampling is employed to reconstruct the image as if the CCD array were composed of contiguous detectors.

4. ***Line loss correction.*** In case of data dropout during transfer from satellite to ground, whole lines may be missing from the image. If no more than three consecutive lines are missing, averaging or repetition of the preceding/following lines may be employed to fill in the gaps (ISRO, 2003b).

It should be noted that band-to-band registration is not applied to Radiometric products; this is particularly important to remember for LISS-III and AWiFS, since the different bands are collected via different telescope assemblies. Photogrammetric software offering support for RESOURCESAT-1 Radiometric products is thus required to account for the fact that the four optical assemblies have different interior orientation parameters and different orientation angles with respect to the spacecraft's attitude sensors. Because this is not the case with most photogrammetric software on the market today, Radiometric products are made available by request only and are not part of the standard product offering.

For those users who are unable to deal with the band-to-band misregistration of Radiometric products, the next option is the Geo product. This is a georectified image, projected onto the surface of the reference ellipsoid and resampled to a consistent grid spacing in a map-projected coordinate system.

Geo products can be created in either a path-oriented or map-oriented grid. In the path-oriented product, the resampling grid is rotated to match as closely as possible the satellite ground track. This minimizes the amount of blackfill in the output image and thus reduces the file size. The map-oriented product uses a resampling grid aligned with the coordinate axes of the map projection.

While Geo products have been resampled to a consistent grid spacing on the ground, they still contain relief displacement. The Orthorectified image product, on the other hand, has been corrected for terrain relief and is thus the most suitable product for users who do not wish to perform their own photogrammetric processing of the imagery.

Data Formats

RESOURCESAT-1 data is available in a number of formats, including Fast Format, GeoTIFF, and LGSOWG. Major features of each data format are described below.

Fast Format. Fast Format is the simplest data format available for RESOURCESAT-1 imagery. Fast Format data consists of a set of raw binary raster files for each image band, along with a header file containing sensor metadata. The format of this header file is described by Mahammad (2002) and lists, among other things:

- Scene ID
- Collection date of the imagery
- Look angle off-nadir from satellite to ground
- Resampling algorithm used
- Number of lines/samples/bands and bits per pixel
- DN-to-radiance conversion coefficients and sensor gain settings
- Map projection parameters
- Scene corner coordinates
- Azimuth and elevation angle of the sun
- Approximate satellite altitude and azimuth of the satellite ground track

Because Fast Format is a very simple format, it is straightforward to implement software support for it. However, very little geometric information is transferred along with the image, making it difficult to use for photogrammetric work.

Several commercial photogrammetric software packages are capable of ingesting RESOURCESAT-1 Fast Format products, since the file format has not changed from IRS-1C and IRS-1D (ISRO, 2003b). If software support for Fast Format is not available, GeoTIFF format data may be more suitable.

GeoTIFF. GeoTIFF format is currently available for Orthorectified and map-oriented Geo products. Nearly all photogrammetric and GIS software supports GeoTIFF, so it is a good choice for those who do not wish to perform any format conversion. The GeoTIFF product contains the same metadata as provided with Fast Format, but in this case the metadata is not supplied as a separate file. Instead, the metadata is contained within the 'ImageDescription' field (TIFF tag number 270) of the GeoTIFF file header. The format of this metadata is the same as that for a Fast Format header file. Therefore, as with Fast Format, very little geometric information is provided with the image.

LGSOWG. The most useful data format for photogrammetric users is LGSOWG, also known as Super Structure format. This format includes a number of ancillary data files that provide such information as ephemeris, attitude, camera-target-sun viewing geometry, focal lengths of the different telescope assemblies, and DN-to-

radiance conversion coefficients. A full description of the RESOURCESAT-1 LGSOWG product format is provided in Mahammad and Jamindar (2002).

RESOURCESAT-1 PHOTOGRAMMETRIC PROCESSING

Photogrammetric software developers who wish to implement support for RESOURCESAT-1 imagery products will be confronted with the task of recovering the satellite-to-ground imaging geometry from the provided sensor metadata. Of the available data formats, the most useful for this purpose is LGSOWG format.

For those wishing to implement a full physical sensor model, LGSOWG format Radiometric products are the best choice. The LGSOWG metadata provides a number of elements describing the physical sensor and collection geometry, including:

- Ephemeris and attitude records given at a 0.125 second time interval
- Camera focal lengths
- Detector integration time
- Roll/pitch/yaw bias angles
- Time at scene center
- 'Map projection' records giving a grid of line/sample coordinates and corresponding lat/lon coordinates, and azimuth/elevation from ground point to satellite and sun

Unfortunately, the provided metadata does not include all parameters needed to describe the physical camera model. It is possible to find published values for some other items in the *IRS-P6 Data User's Manual* (ISRO, 2003b), for instance, the size of the CCD elements. However, some other required elements are not listed at all, including lens distortion parameters and the positions of the CCD arrays on the focal plane. In spite of this, the provided metadata is useful as a starting point, and it would be possible to estimate the unknown parameters if suitable ground control is available. Physical sensor models for LISS-III and AWiFS should include separate interior orientation parameters for each band, as they employ different telescope assemblies. Developers wishing to implement a physical sensor model using LGSOWG metadata can find a description of the coordinate systems used for the ephemeris and attitude records in Mahapatra et al. (2004).

As an alternative to estimating the parameters of a physical sensor model for the Radiometric product, it is also possible to reconstruct the view geometry for Geo images in a way that permits representation by Rational Polynomial Coefficients (RPCs). This has the advantage of allowing the ingest of RESOURCESAT-1 imagery into existing photogrammetric software packages with a minimum of programming effort on the part of the developer. Furthermore, it will be shown in later sections that this approach allows the user to obtain very good positional accuracy for all three sensors, provided a modest amount of ground control is available. The following sections describe how to recover the ground-to-satellite view geometry from LGSOWG format metadata.

Image Geometry Reconstruction

Reconstruction of the viewing geometry from sensor metadata allows the user to compute, for any ground point, the corresponding line and sample coordinates in the image. If the relationship between ground space and image space is known, it is then possible to extract meaningful geometric information from the image.

RESOURCESAT-1 Geo images in LGSOWG format are the best candidate for reconstruction of the image geometry. Unlike Radiometric scenes, the Geo product has already been georectified and all bands are resampled into a common grid on the mapping plane.

The key feature of LGSOWG format data that makes it more useful than other formats is the so-called 'Map Projection' segment of the leader file (Mahammad and Jamindar, 2002). This segment alone contributes nearly all the information needed to reconstruct the view geometry.

The Map Projection records in the LGSOWG leader file list, for a grid of points covering the image, the following elements:

- Line and sample coordinates of the grid point in the image;
- Latitude and longitude where the ray from this grid point strikes the surface of the reference ellipsoid;
- Azimuth and elevation from the ground point to the satellite; and
- Azimuth and elevation from the ground point to the sun.

The line and sample coordinates provided in the Map Projection record start at 1 rather than 0; that is, the upper-left pixel in the image has sample and line coordinates of (1,1). For UTM products, the latitude and longitude values are replaced by Northing and Easting. Parameters are also provided in the Map Projection record to describe

the map projection and ellipsoid used for the product. The datum used is not currently indicated in the Map Projection record, so the user must consult with the data provider for details.

The azimuth and elevation values listed in the Map Projection records are not, as one might expect, based on a Local Space Rectangular system with origin at the grid point. Instead, they are spherical angles, computed using formulae presented in Buglia (1988). The elevation angle *el* is based on the geometry depicted in Figure 1:

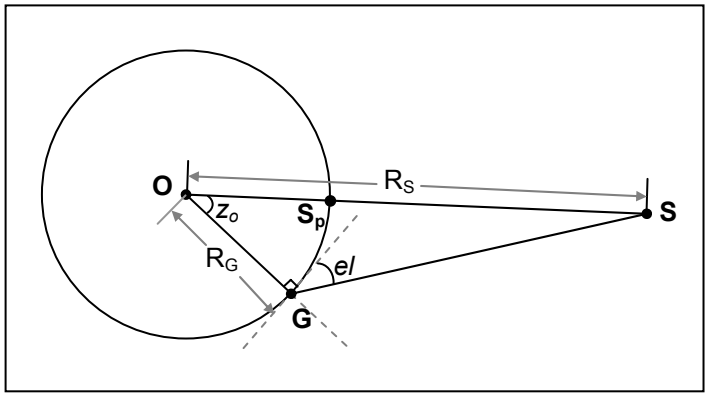

Figure 1. Geometry for calculation of LGSOWG elevation angle from ground to satellite

where:

G is the grid point;
R_G is the distance of **G** from **O**, the origin of the coordinate system;
S is the satellite point;
R_s is the distance of **S** from **O**;
$\mathbf{S_p}$ is the sub-satellite ground point on the surface of the sphere of radius R_G;
el is the elevation angle measured from the perpendicular of **OG** to **S**; and
z_o is the angle subtended at **O** from **S** to **G**.

The azimuth *az* is then computed as a spherical angle on the surface of a sphere with radius R_G, as shown in Figure 2(a). A closeup of the spherical triangle $\mathbf{N\text{-}G\text{-}S_p}$ is shown in Figure 2(b):

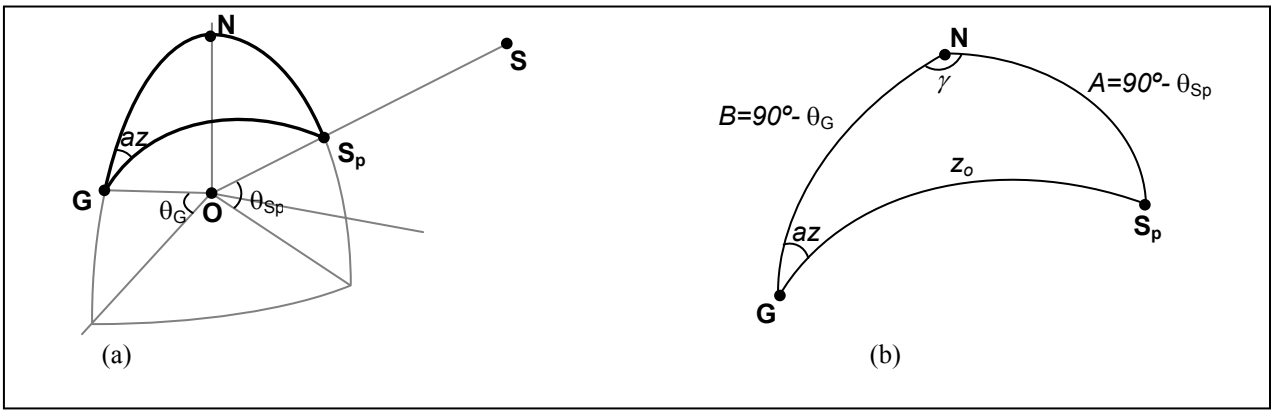

Figure 2. Geometry for calculation of LGSOWG azimuth from ground to satellite

where:

N is the North pole of the sphere of radius R_G;
θ_G, θ_{Sp} are the geocentric latitudes of **G** and $\mathbf{S_p}$, respectively; and
A, B, γ are elements of the spherical triangle, which will be used in later calculations.

One can see from Figures 1 and 2 that the spherical azimuth and elevation angle alone are not enough to define the position of, or even the direction to, the satellite. It is necessary to know R_s in order to compute z_o, so that

enough elements are available to complete the spherical triangle. Fortunately, an average value for R_s can be derived from the Ephemeris segment of the LGSOWG leader file.

Computation of the satellite position corresponding to a grid point in the Map Projection records can thus be performed in the following sequence of steps:

1. Use the Ephemeris records to compute the average distance R_S of the satellite from the origin of the coordinate system.
2. From the listed grid point position λ_G, ϕ_G for point **G**, compute the Cartesian coordinates X_G, Y_G, Z_G. Assume an ellipsoidal height h_G of zero. In the case of UTM products, the grid point position will have to be reprojected from Easting and Northing to λ_G, ϕ_G.
3. Compute the distance R_G of the grid point from the origin of the coordinate system. R_G will be the radius of the sphere used for spherical angle calculations later on.
4. From the given elevation angle el, calculate the angle z_o using equation (1):

$$z_o = 90° - el - \sin^{-1}\left[\frac{R_G}{R_S}\sin(el + 90°)\right] \tag{1}$$

5. Calculate the geocentric latitude θ_G of point **G** using equation (2):

$$\theta_G = \tan^{-1}\left[\frac{Z_G}{\sqrt{{X_G}^2 + {Y_G}^2}}\right] \tag{2}$$

6. Compute elements of the spherical triangle to solve for γ, the longitude difference from G to the sub-satellite ground point Sp.

$$\alpha = \begin{cases} az & az \le 180° \\ 360° - az & az > 180° \end{cases} \tag{3}$$

$$B = 90° - \theta_G \tag{4}$$

$$A = \cos^{-1}(\cos B \cdot \cos z_o + \sin B \cdot \sin z_o \cdot \cos\alpha) \tag{5}$$

$$\gamma = \cos^{-1}\left[\frac{\cos z_o - \cos A \cdot \cos B}{\sin A \cdot \sin B}\right] \tag{6}$$

7. Compute geocentric latitude and longitude of sub-satellite point $\mathbf{S_p}$ using equations (7) and (8).

$$\theta_{Sp} = 90° - A \tag{7}$$

$$\lambda_{Sp} = \begin{cases} \lambda_G + \gamma & az \le 180° \\ \lambda_G - \gamma & az > 180° \end{cases} \tag{8}$$

8. Compute Cartesian coordinates X_S, Y_S, Z_S of the satellite point **S** using equation (9).

$$\begin{aligned} X_S &= R_S \cdot \cos\lambda_{Sp} \cdot \cos\theta_{Sp} \\ Y_S &= R_S \cdot \sin\lambda_{Sp} \cdot \cos\theta_{Sp} \\ Z_S &= R_S \cdot \sin\theta_{Sp} \end{aligned} \tag{9}$$

Once the position **S** of the satellite has been determined, it is a trivial task to compute the line of sight from ground to satellite. Knowledge of the line of sight direction allows the user to compute the direction of relief displacement in the Geo image, making orthorectification possible.

ACCURACY ASSESSMENT

Using the steps outlined in the previous section, the Map Projection records of the LGSOWG file can be used to generate a 3D point cloud representing the view geometry. At each grid point, the line-of-sight vector from ground to image is used to calculate longitude and latitude at a range of different height values covering the terrain. Given longitude, latitude and height values for a 3D grid covering the image and terrain elevation extents, rational polynomial coefficients (RPCs) describing the view geometry can be computed for the scene as described in Grodecki (2001).

If RPCs are computed for the scene and the LGSOWG raster data is converted to a generic image format such as TIFF, it then becomes possible to ingest RESOURCESAT-1 Geo scenes into a number of commercial photogrammetry packages using an RPC-based model. In this study, the so-called 'IKONOS' geometric correction model in ERDAS Imagine (Leica Geosystems, 2002), which requires an image file and associated text file containing rational polynomial coefficients, was used to perform the accuracy assessment. This model allows the inclusion of image-space polynomial correction terms to remove systematic errors in the image, as described in Grodecki and Dial (2003).

In order to determine the geometric accuracy of LISS-IV scenes, Digital Ortho Quadrangles (DOQs) from the United States Geological Survey (USGS) were used as map control. Elevations for the control points were derived from the USGS National Elevation Dataset (NED). For each LISS-IV scene, at least 20 control points were measured and the difference in measured vs. predicted sample and line locations (ΔS and ΔL) were computed. Next, an image space adjustment polynomial was introduced, with degree varying from 0 (offset only) to 2 (quadratic terms). Table 4 illustrates the accuracy improvement obtained with different degrees of adjustment polynomial, with line and sample errors scaled to meters.

Table 4. LISS-IV block adjust results

Scene	*Uncorrected scene*				*0th order polynomial correction*		*1st order polynomial correction*		*2nd order polynomial correction*	
	ΔS_{avg} [m]	ΔL_{avg} [m]	$\sigma_{\Delta S}$ [m]	$\sigma_{\Delta L}$ [m]	$\sigma_{\Delta S}$ [m]	$\sigma_{\Delta L}$ [m]	$\sigma_{\Delta S}$ [m]	$\sigma_{\Delta L}$ [m]	$\sigma_{\Delta S}$ [m]	$\sigma_{\Delta L}$ [m]
L4M250034C	-240.5	380.9	16.5	51.5	16.5	51.5	2.0	1.9	1.7	1.8
CE90:				**465.2**		**116.1**		**5.9**		**5.2**
L4M250036C	-258.7	368.5	18.4	59.0	18.4	59.0	4.9	3.9	4.7	3.5
CE90:				**469.4**		**132.7**		**13.4**		**12.6**
L4M250044C	-292.1	407.2	15.6	48.1	15.6	48.1	1.6	2.2	1.4	1.8
CE90:				**512.8**		**108.6**		**5.8**		**4.9**
L4m260044C	-353.3	417.3	24.1	69.3	24.1	69.3	2.1	2.3	2.0	2.0
CE90:				**568.9**		**157.4**		**6.7**		**6.1**
L4M260045A	-351.2	404.7	22.6	67.5	22.6	67.5	2.4	2.0	2.1	1.5
CE90:				**557.2**		**152.7**		**6.8**		**5.4**
L4M269042D	-241.5	-17.7	20.7	68.6	20.7	68.6	2.2	2.1	2.0	1.6
CE90:				**286.9**		**153.7**		**6.6**		**5.4**
L4M269043D	-182.9	335.1	18.9	57.4	18.9	57.4	3.0	3.6	2.3	2.7
CE90:				**403.2**		**129.7**		**10.1**		**7.7**
L4M278042A	-223.0	381.3	21.6	68.1	21.6	68.1	2.1	2.2	1.9	1.9
CE90:				**467.6**		**153.4**		**6.4**		**5.8**
L4M278042C	-222.8	369.8	23.2	67.9	23.2	67.9	1.9	2.0	1.8	1.7
CE90:				**458.3**		**153.9**		**5.9**		**5.3**

The results show that by using a first-order polynomial correction, LISS-IV scenes can be corrected to a high degree of accuracy. Use of a second-order polynomial correction is not warranted, as the extra accuracy improvement is minimal in relation to the pixel size. The achievable accuracy is generally better than 10 meters CE90 for the scenes tested, which in this case is approximately the accuracy level of the map control used (12 m CE90).

Figure 3 shows the observation residuals for a typical LISS-IV scene when only a 0^{th} order correction polynomial is used, illustrating why a first-order adjustment polynomial is required. The pixel size for this scene was 5 meters.

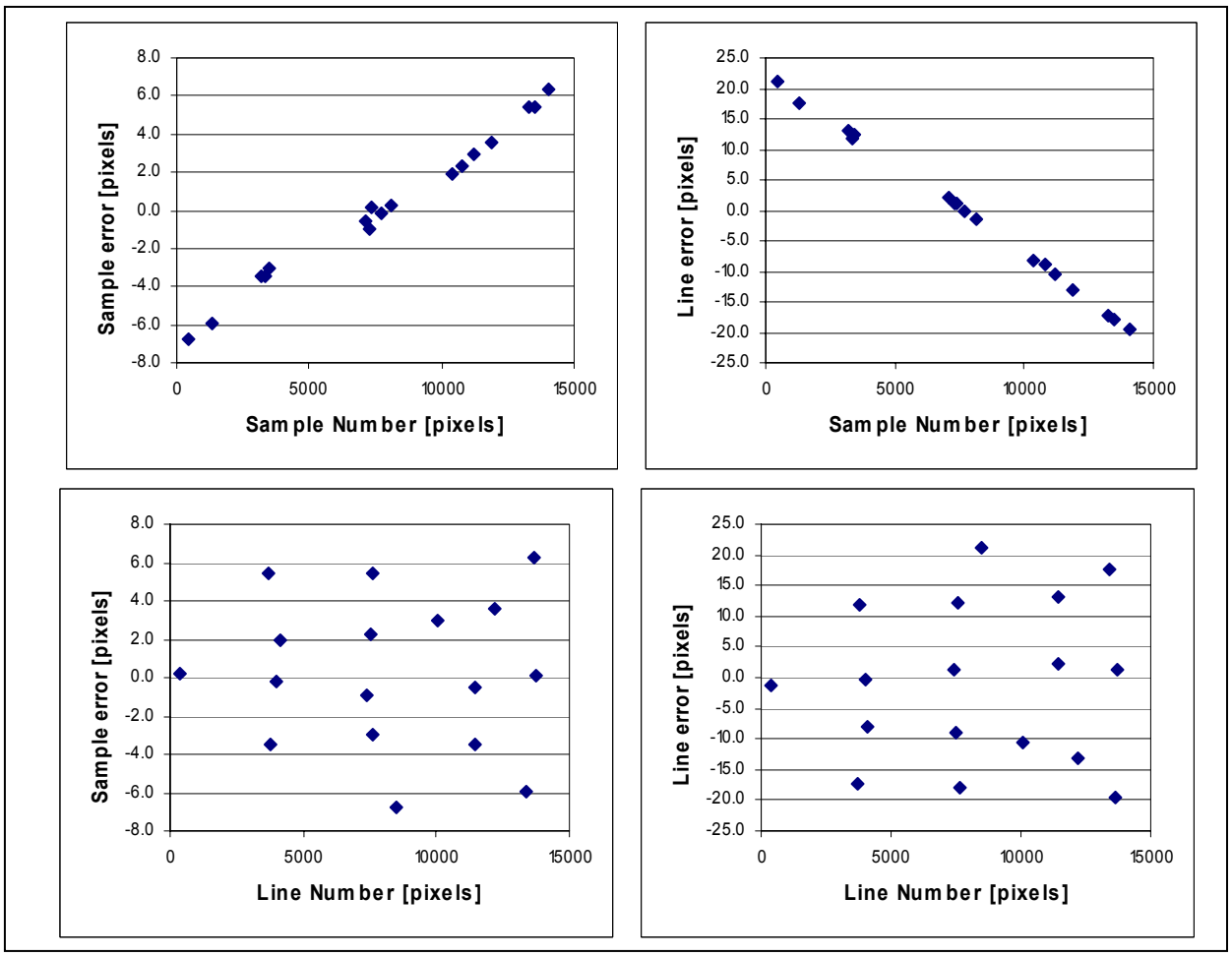

Figure 3. Observation residuals for scene L4M269042D (0th order polynomial correction)

Errors in both sample and line are both strongly correlated with the sample number, which in path-oriented scenes corresponds to the cross-track direction. The same trend was present in all nine of the LISS-IV scenes tested, suggesting perhaps a bias in yaw or in the orientation of the detector array on the focal plane.

With LISS-III data, the accuracy improvement gained when going from a 0th-order correction to a 1st-order correction is smaller but still significant, as shown in Table 5. Achievable accuracy for LISS-III is generally better than 30 m CE90 when a first-order polynomial correction is used.

Table 5. LISS-III block adjust results

Scene	*Uncorrected scene*				*0th order polynomial correction*		*1st order polynomial correction*		*2nd order polynomial correction*	
	ΔS_{avg} [m]	ΔL_{avg} [m]	$\sigma_{\Delta S}$ [m]	$\sigma_{\Delta L}$ [m]	$\sigma_{\Delta S}$ [m]	$\sigma_{\Delta L}$ [m]	$\sigma_{\Delta S}$ [m]	$\sigma_{\Delta L}$ [m]	$\sigma_{\Delta S}$ [m]	$\sigma_{\Delta L}$ [m]
L-3249045	-273.8	146.6	11.5	17.5	11.5	17.5	9.2	6.3	8.0	6.0
CE90:				**313.8**		**44.9**		**24.0**		**21.6**
L-3250034	-273.0	175.5	11.1	20.4	11.1	20.4	9.1	8.8	8.2	8.5
CE90:				**328.3**		**49.8**		**27.2**		**25.3**
L-3260045	-402.7	215.4	9.4	15.6	9.4	15.6	7.6	6.5	6.6	6.4
CE90:				**458.4**		**39.0**		**21.4**		**19.8**
L-3260046	-391.7	249.8	13.1	27.3	13.1	27.3	8.1	12.8	7.8	12.1
CE90:				**469.1**		**64.9**		**32.5**		**30.9**
L-3279042	-355.1	251.7	10.2	17.3	10.2	17.3	5.9	5.8	5.7	5.6
CE90:				**437.4**		**43.1**		**17.7**		**17.2**
L-3288041	-325.1	91.1	9.7	13.8	9.4	14.4	7.6	5.5	6.4	5.5
CE90:				**339.5**		**36.8**		**20.2**		**18.2**

As with LISS-IV, all scenes showed similar trends as a function of sample number; both sample and line errors varied linearly with sample number, with a range of 2-4 pixels across the width of the scene. Observation residuals are plotted versus sample number in Figure 4, where the image pixel size is 20 meters.

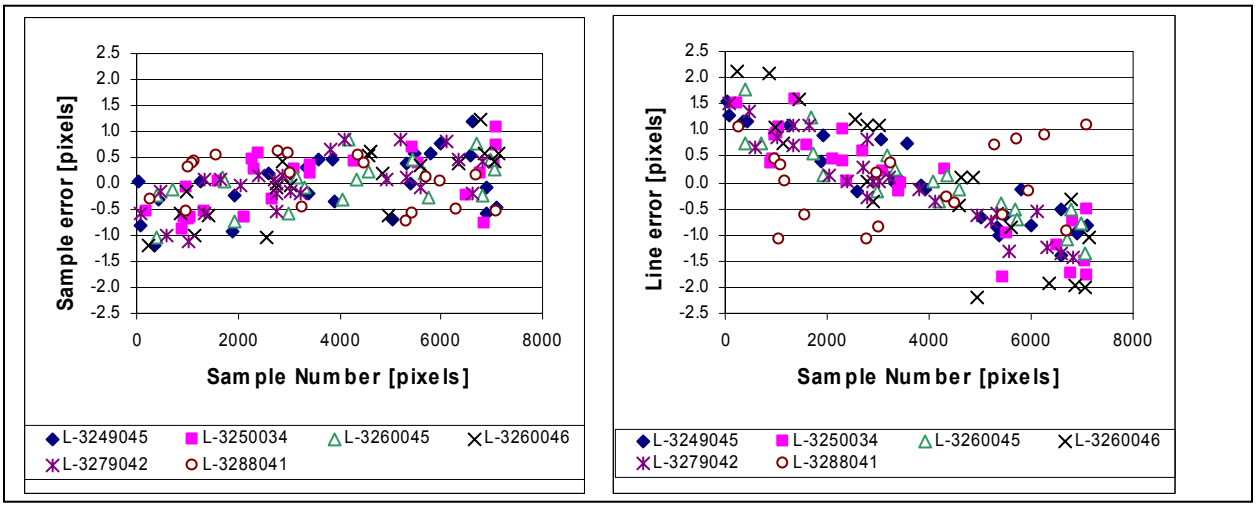

Figure 4. Observation residuals vs. sample for LISS-III scenes (0th order polynomial correction)

Finally, the same procedure was performed for eight AWiFS scenes, four collected using the AWiFS-A camera (scene names ending with 'A' and 'C') and four from AWiFS-B (scene names ending with 'B' and 'D'). In this case, there is a noticeable difference between the AWiFS-A scenes and the AWiFS-B scenes; AWiFS-B is well-modeled with a first-order polynomial correction, while AWiFS-A requires second-order correction terms.

Table 6. AWiFS block adjust results

Scene	*Uncorrected scene*				*0th order polynomial correction*		*1st order polynomial correction*		*2nd order polynomial correction*	
	ΔS_{avg} [m]	ΔL_{avg} [m]	$\sigma_{\Delta S}$ [m]	$\sigma_{\Delta L}$ [m]	$\sigma_{\Delta S}$ [m]	$\sigma_{\Delta L}$ [m]	$\sigma_{\Delta S}$ [m]	$\sigma_{\Delta L}$ [m]	$\sigma_{\Delta S}$ [m]	$\sigma_{\Delta L}$ [m]
AWF250045A	-615.7	204.3	137.4	24.5	137.4	24.5	58.2	16.1	11.4	15.5
CE90:				**714.5**		**299.6**		**129.6**		**41.3**
AWF250045C	-562.2	236.8	118.8	20.0	118.8	20.0	62.2	12.9	12.7	12.3
CE90:				**662.5**		**258.5**		**136.3**		**37.9**
AWF260044C	-665.5	252.3	118.4	16.0	118.4	16.0	52.3	13.2	14.2	12.6
CE90:				**756.5**		**256.4**		**115.7**		**40.8**
AWF273046C	-600.0	189.2	131.7	16.3	131.7	16.3	53.6	11.7	12.4	9.5
CE90:				**690.6**		**284.8**		**117.8**		**33.5**
AWF250035D	188.9	354.7	153.9	18.4	153.9	18.4	12.9	14.6	8.5	14.5
CE90:				**521.6**		**332.5**		**41.8**		**36.1**
AWF260044D	65.4	512.8	175.0	25.1	175.0	25.1	15.2	9.8	12.6	8.1
CE90:				**641.3**		**379.5**		**38.7**		**32.2**
AWF287040B	204.4	365.6	206.5	17.6	206.5	17.6	19.9	17.5	18.4	14.9
CE90:				**610.9**		**444.7**		**56.8**		**50.7**
AWF288046B	-38.8	244.5	71.9	16.2	71.9	16.2	14.3	12.3	13.1	11.7
CE90:				**293.8**		**158.2**		**40.5**		**37.7**

A plot of the line and sample residuals as a function of sample illustrates the difference between the two cameras (see Figure 5 and Figure 6; pixel sizes are 50 meters). The AWiFS-B camera shows a strong linear trend of sample error vs. sample number, and perhaps a slight trend in line error vs. sample number. Because all scenes show a linear trend in sample error with the same slope, this is most likely due to miscalibration of focal length. This causes a scale error in the cross-track direction, which is easily absorbed by the first-order polynomial

correction terms. The typical accuracy achieved when using a first-order polynomial correction was better than 60 meters CE90.

Observation residuals from the AWiFS-A scenes (Figure 6) reveal a systematic but nonlinear relation between sample error and sample number. This could be due to residual radial lens distortion or other factors; in any case, the trend is adequately modeled by a second-order polynomial correction. This yields a positional accuracy better than 50 meters CE90 for the scenes tested.

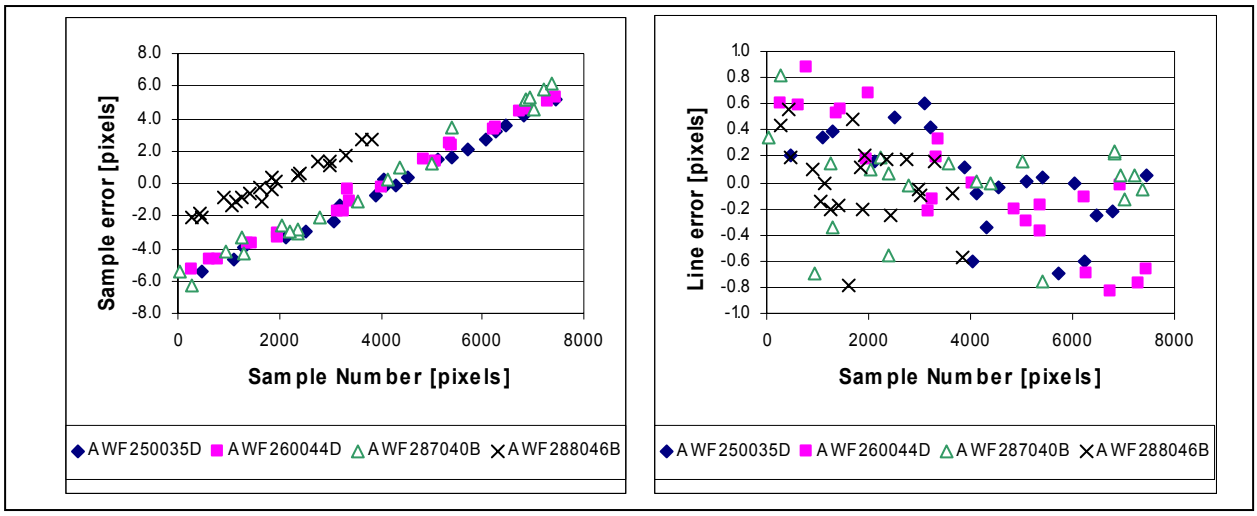

Figure 5. Observation residuals vs. sample for AWiFS-B scenes (0th order polynomial correction)

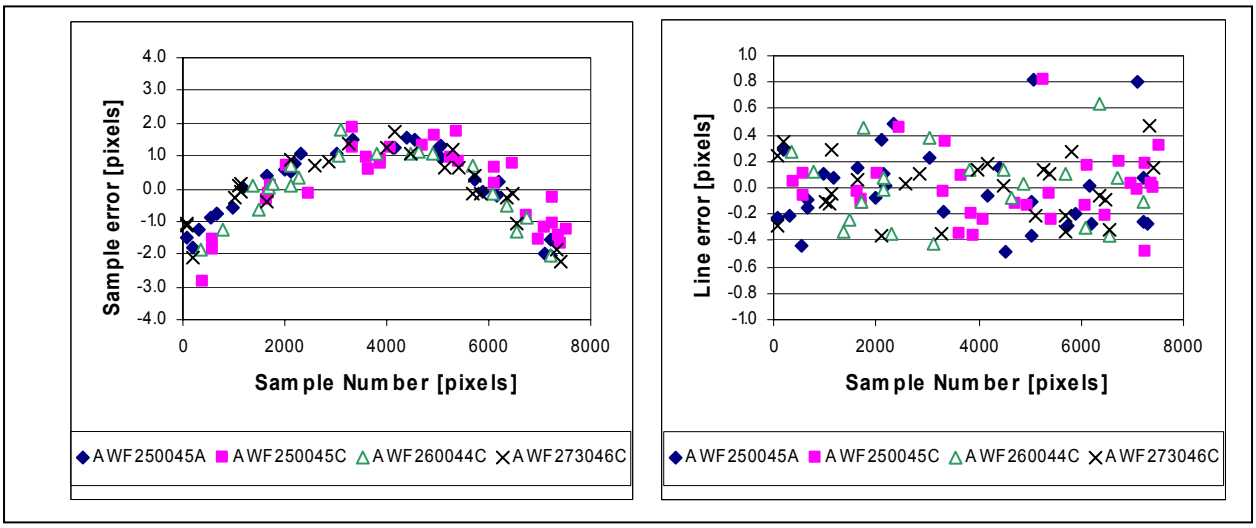

Figure 6. Observation residuals vs. sample for AWiFS-A scenes (0^{th} order polynomial correction)

Based on these results, it can be seen that Geo scenes from all sensors exhibit geometric errors that could likely be reduced by recalibration of physical camera parameters. These effects result in low positional accuracy for uncorrected scenes, but the errors can be quite well modeled by introducing a polynomial correction in image space. When the correction terms are introduced, the resulting accuracies are quite good, considering the spatial resolution of the sensors.

CONCLUSIONS

RESOURCESAT-1, the latest of ISRO's series of remote sensing satellites, provides both data continuity and a number of improvements over its predecessors IRS-1C and IRS-1D. This paper has provided an overview of the sensors aboard RESOURCESAT-1 and a description of some of the data products available.

For photogrammetric software developers who wish to incorporate RESOURCESAT-1 support into their products, imagery should be obtained in LGSOWG format. This format provides much more metadata describing the imaging geometry than do the other available data formats. Developers who wish to develop a physical sensor model for the imagery should use imagery processed to the Radiometric level; they must be aware, however, that LISS-III and AWiFS collect imagery using different telescope assemblies for the different bands, and not all of the physical camera parameters are provided with scene metadata.

For those who wish to use RESOURCESAT-1 imagery in existing commercial software packages, an algorithm has been presented illustrating how the LGSOWG metadata for path-oriented Geo scenes can be used to recover imaging geometry and thus generate RPCs for the imagery. Many commercial photogrammetric software packages support the use of RPCs to describe imaging geometry, so this may be the best solution for many customers who wish to perform their own block adjustment and orthorectification.

The geometric accuracy of RESOURCESAT-1 imagery has been evaluated using the RPC model in ERDAS Imagine's Geometric Correction tool. For the scenes tested, the initial geometric accuracy turned out to be rather poor; most scenes fell within the 500-700 m CE90 range. Examination of patterns in the observation residuals, however, revealed that this was likely due to mis-calibration of some physical sensor parameters. The residual errors exhibited very systematic patterns that could be easily modeled using a low-order polynomial correction (first-order for LISS-IV, LISS-III and AWiFS-B, and second-order for AWiFS-A). When polynomial correction terms are incorporated, the resulting accuracy is very good: typically better than 10 m CE90 for LISS-IV, better than 30 m CE90 for LISS-III, and better than 60 m CE90 for AWiFS.

REFERENCES

Buglia, J. (1988). *Compilation of Methods in Orbital Mechanics and Solar Geometry.* NASA Reference Publication 1204, Langley Research Center, Hampton, Virginia.

Grodecki, J. (2001). IKONOS stereo feature extraction—RPC approach. Proceedings of ASPRS 2001 Conference, St. Louis, April 23-27, 2001.

Grodecki, J. and G. Dial (2003). Block adjustment of high-resolution satellite images described by rational polynomials. *Photogrammetric Engineering & Remote Sensing*, 69(1):59-68.

ISRO (2003a). PSLV launches RESOURCESAT-1 (IRS-P6). ISRO press release, http://www.isro.org/pressrelease/Oct17_2003.htm, retrieved 15 November 2004.

ISRO (2003b). *IRS-P6 Data Users' Handbook*, NRSA Report No. IRS-P6/NRSA/NDC/HB-10/03, October 2003, Hyderabad, India. http://www.nrsa.gov.in/engnrsa/p6book/handbook/handbook.pdf, retrieved February 2004.

Leica Geosystems (2002). *ERDAS Imagine 8.6 On-Line Help Manual*. Leica Geosystems, GIS & Mapping Division, Atlanta, Georgia.

Mahammad, S. (2002). *IRS-1C/1D/P6 Digital Data Products Format for Revision C Fast Format Products.* Space Application Center (SAC) Report No. IRS-P6/DP/SAC/SIIPA/SIPG/TN-05, May 2002, Ahmedabad, India.

Mahammad, S. and V. Jamindar (2002). *IRS-P6 LGSOWG (Super Structure) Digital Data Products Format*. SAC Report No. SAC/DPSD/SIPG/IRS-P6 FORMAT/TN-10, August 2002, Ahmedabad, India

Mahapatra, A., R. Ramchandran, and R. Krishnan (2004). Modeling the uncertainty in orientation of IRS-1C/1D with a rigorous photogrammetric model. *Photogrammetric Engineering & Remote Sensing*, 70(8):939-946.

NRSA (National Remote Sensing Agency, Government of India) (1995). *IRS-1C Data Users' Handbook*. NRSA Report No. NDC/CPG/NRSA/IRS-1C/HB/Ver 1.0, September 1995, Hyderabad, India.

NRSA (1997). *IRS-1D Data Users' Handbook*. NRSA Report No. IRS-1D/NRSA/NDC/HB-12/97, December 1997, Hyderabad, India.

NRSA (2004). Future Missions. http://www.nrsa.gov.in/engnrsa/products/futuremissions.html, retrieved 15 November 2004.